Hindawi
Geofluids
Volume 2023, Article ID 3701163, 9 pages
https://doi.org/10.1155/2023/3701163

WILEY | Hindawi

Research Article

Pore Structure and Permeability Variations during Gas Displacement in Unconsolidated Sandstone Reservoirs through CT Reconstruction Analysis

Yuqiang Zha, Bao Cao, Fengying Li, Qing Ye, Shaopeng Zhu, Wei Zhou, and Runfu Xiong

CNOOC China Limited, Hainan Branch, Haikou 570311, China

Correspondence should be addressed to Yuqiang Zha; zhayq@cnooc.com.cn

Received 14 February 2023; Revised 15 March 2023; Accepted 21 April 2023; Published 29 May 2023

Academic Editor: Shiling Zhang

The continuous gas displacement in unconsolidated sandstone gas reservoirs will necessarily result in the pore structure and rock permeability variations, which cannot be neglected in the gas development process. However, the variations have not been comprehensively addressed yet, especially for the rock structure in pore scale. This work presented the quantitative results of pore structure in microscale and permeability variations during gas displacement in unconsolidated sandstone reservoirs through computed tomography (CT) reconstruction analysis. The results indicated that a more than 3% increase in porosity after gas displacement resulted from the enlargement of the pore and throat with a diameter of more than 20 μm and 3 μm, respectively, owing to the release and migration of clay and fine particles, in spite of the distribution frequency decline of both pore and throat with a small diameter. The pore connectivity would be enhanced by the increase of the connected pores as well as the enlargement of the pore and throat sizes. However, the pore-throat coordination number could only change with slight improvement. In terms of permeability and relative permeability changes with pore structure, the improvement of permeability after gas displacement was higher than that of porosity, and the continuous gas displacement would broaden gas-water flow region and lower irreducible water saturation and residual gas saturation, and then, the equal phase relative permeability point would shift to the right. These investigations will contribute to more accurate reserve evaluation and productivity prediction.

1. Introduction

Natural gas as a clean energy resource has been wildly applied in various fields, including heating, power generation, automobile fuel, food processing, steel industry, chemical refining, hydrogen production, and synthetic ammonia [1–3]. More attention has been paid to the exploration and development of natural gas. How to get a better development effect becomes crucial to extracting more resources. Among all types of natural gas reservoirs in China, the development of unconsolidated sandstone gas reservoirs such as the gas fields in the Qaidam Basin, western South China Sea, and Baoshan Basin [4–6] has been confronted with kinds of problems including sand production, water channeling, and more serious heterogeneity [7–9], further affecting the productivity. These problems result from the changes in the petrophysical properties of the unconsolidated sandstone, especially the changes in the pore structure and permeability [10, 11].

The changes are primarily on account of the release and migration of rock mineral particles including clay and fine particles in the long-term flow of gas and water [12, 13]. The continuous fluid flow in porous media, especially in the unconsolidated sandstone, will enlarge and also block the pore throat, further changing the permeability [14, 15]. The pore structure and permeability variations should be comprehensively addressed so as to get a better understanding of them. However, the research to date mostly concentrates on the macroscopic time-dependent porosity and permeability evolution in core and field scale including physical and numerical simulation [16–18], especially for oil reservoirs [19–22]. And the macroscopic investigation

Table 1: Mineralogical compositions of the core.

Quartz (%)	Potassium feldspar (%)	Plagioclase (%)	Calcite (%)	Montmorillonite (%)	Illite (%)	Kaolinite (%)	Chlorite (%)
55.5	8.1	14.4	1.3	4.60	6.00	5.84	4.26

Table 2: Petrophysical properties of the core samples.

Sample no.	Gas permeability (mD)	Porosity (%)	Length (cm)	Diameter (cm)	Pore volume (cm^3)
$1^{\#}$	/	35.71	1.10	0.60	0.11
$2^{\#}$	39.24	34.22	6.01	2.49	10.01

will not provide a revealing insight into the microscope evolution. The general ways to investigate the pore structure include centrifuge, mercury intrusion, nitrogen adsorption, nuclear magnetic resonance (NMR), and computed tomography (CT) [23–27]. All of them can reflect the pore size distribution but cannot physically present the spatial pore structure except CT [28]. With the rapid development of experimental detection technology, the CT technology with higher scanning precision and better reconstruction algorithm makes it easy to provide a deep insight into the changes in pore scale [29, 30]. It has been increasingly utilized in the fluid distribution and pore structure reconstruction [31, 32]. By the CT reconstruction analysis, the parameters can be characterized in pore scale, including the number and geometry of pore and throat, 3D pore structure, and pore connectivity [33, 34]. The changes in pore scale can further clarify the changes in macroscopic porosity and permeability. However, rare research has been conducted to investigate pore structure and permeability variations during gas displacement through CT reconstruction analysis.

Therefore, this work conducted the quantitative evaluations of pore structure in microscale and permeability variations during gas displacement in unconsolidated sandstone reservoirs by means of CT reconstruction analysis. Firstly, the number and size distribution of the pore and throat were evaluated to probe into the pore structure variations after gas displacement. Then, the pore connectivity was investigated from the aspects of the changes of connected pores and pore-throat coordination number. Eventually, the changes in the macroscopic porosity and permeability including relative permeability were further evaluated and clarified by the variations of the structure and connectivity in the pore scale. The comprehensive investigations will provide a deeper insight into the rock petrophysical property changes in the gas displacement process in unconsolidated sandstone gas reservoirs and contribute to more accurate reserve evaluation and productivity prediction.

2. Experimental Section

2.1. Materials. The rock cores used in the experiments were obtained with a water saturation of 0.46 from the unconsolidated sandstone gas reservoir at a depth of 1414.73 m. The XRD analysis was carried out on an X-ray diffractometer (TD-3500, Tongda Science & Technology Co., Ltd., China) to determine the compositions of the core as shown in Table 1. Due to the loose structure of the rock sample, the core samples were drilled out by liquid nitrogen freezing technology rather than the common treatment. Two types of the core samples were drilled out to investigate the pore structure by CT reconstruction and clarify the gas-water permeability. The permeability and porosity of each sample were tested using an automated permeameter-porosimeter (AP-608, Coretest Systems, USA). The petrophysical properties of the core samples are listed in Table 2.

2.2. Instruments. The instruments used in the displacement experiments mainly included an ISCO pump, intermediate container, flow meter, pressure sensor, nitrogen bottle, confining pressure system, high-resolution micronano CT scanner (nanoVoxel-4000, Tianjin Sanying Precision Instrument Co., Ltd., China), and core holder as shown in Figure 1. The XRD analysis was carried out on an X-ray diffractometer (TD-3500, Tongda Science & Technology Co., Ltd., China) to determine the compositions of the core. The porosity and permeability of the core sample were tested using an automated permeameter-porosimeter (AP-608, Coretest Systems, USA).

2.3. Methods and Procedures

2.3.1. Gas Displacement Experiments. The displacement experiments were carried out using the instruments as shown in Figure 1. The experimental procedures can be described as follows: (1) the core sample was cleaned and dried. (2) The core sample was saturated by the 3.0 wt.% KI solution, further aged for 24 h at 85°C. And then, it was scanned by micronano CT to reconstruct the pore structure. (3) The gas displacement was conducted with the gas injected into the sample along the longitudinal axis at an inlet pressure of 0.2 MPa at a flow rate of 5~7 mL/min with a confining pressure of 0.8 MPa. (4) The sample was scanned by micronano CT to reconstruct the pore structure after injecting a certain pore volume (PV) (500 PV and 1000 PV). (5) According to the CT scanning results, the reconstruction analysis was carried out to obtain the pore and throat parameters before and after gas displacement.

Additionally, the gas-water relative permeability measurements were conducted by a nonsteady state method using the same instruments except the CT scanner as the literature [35].

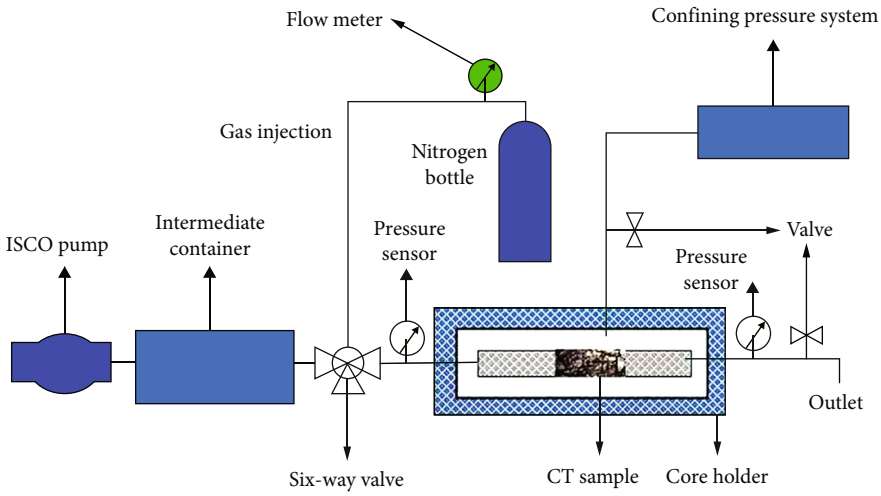

Figure 1: Instruments and procedures of displacement experiments.

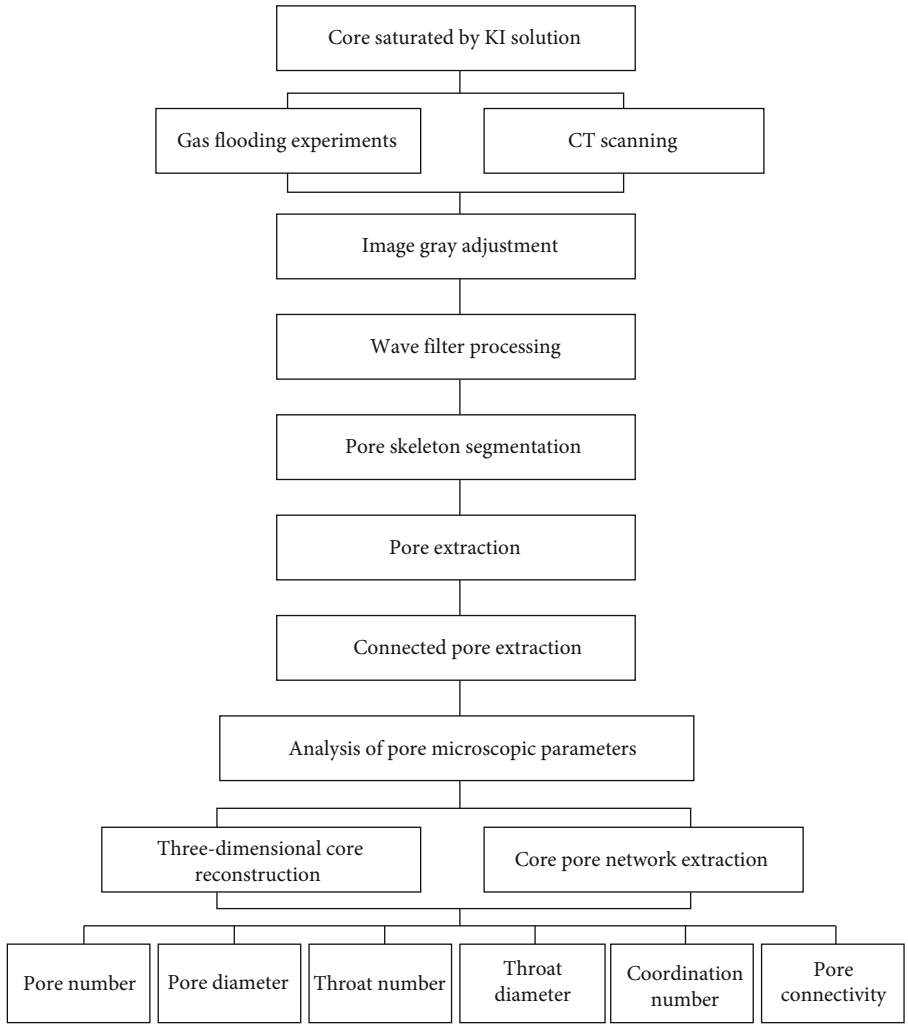

Figure 2: Procedures of CT reconstruction analysis.

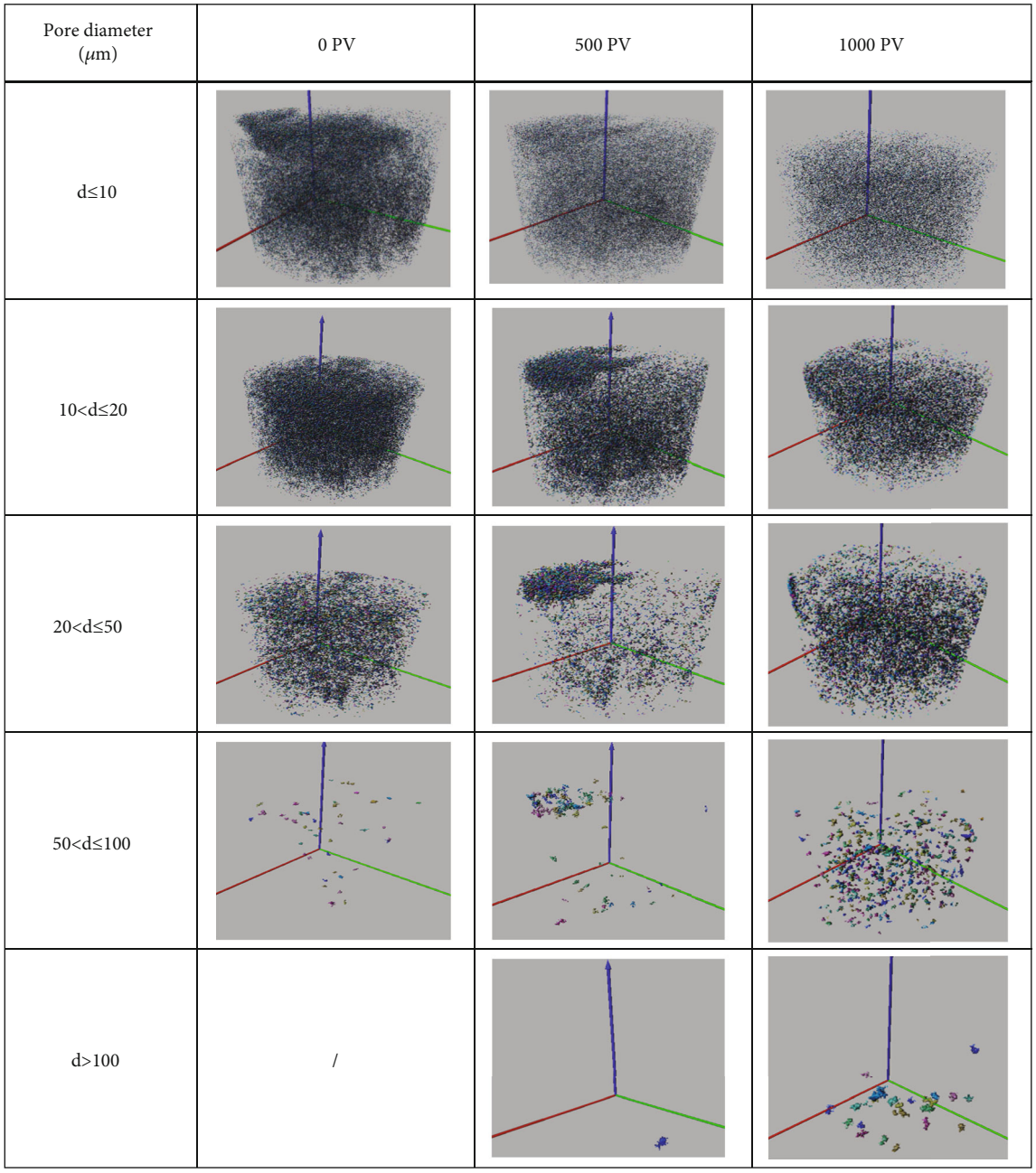

Figure 3: Structure variations of pores of different sizes before and after gas displacement.

2.3.2. CT Reconstruction Analysis. The pore structure was analyzed by CT reconstruction. The reconstruction analysis procedures for the core sample before and after gas displacement are just as shown in Figure 2, mainly including several procedures as follows:

(1) *CT Scanning*. The core sample was scanned by the nanoVoxel-4000 to obtain the high-resolution images

(2) *Data Reconstruction*. The scanning data was processed by algorithm reconstruction and image rectification using the reconstruction software Voxel Studio Recon, including image gray adjustment and wave filter processing

(3) *Data Analysis*. The reconstructed data was then analyzed by the image analysis software such as Volume Graphics Studio Max, FEI Avizo, SYPI-core, and Voxel Studio Render. The analyzed parameters mainly included the number and size of pore and throat, coordination number, and pore and throat connectivity

3. Results and Discussions

3.1. Effects of Gas Displacement on Pore Size. The core sample $1^{\#}$ was used to investigate the pore structure variations. The structures of pores of different sizes in the core sample before and after gas displacement were reconstructed

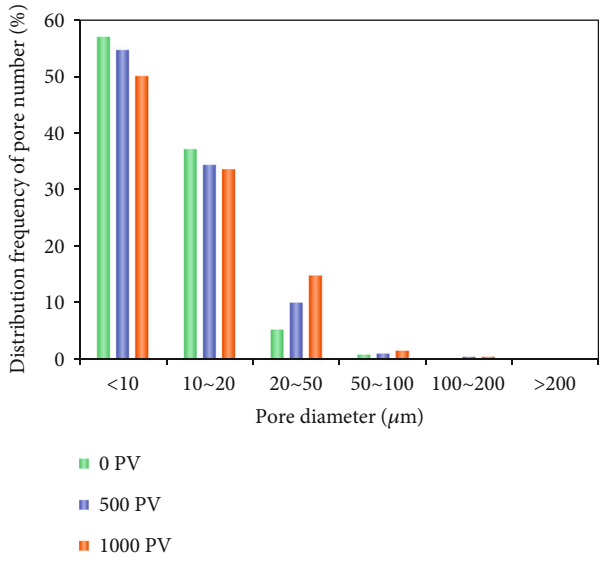

Figure 4: Number distribution frequencies of pores of different sizes before and after gas displacement.

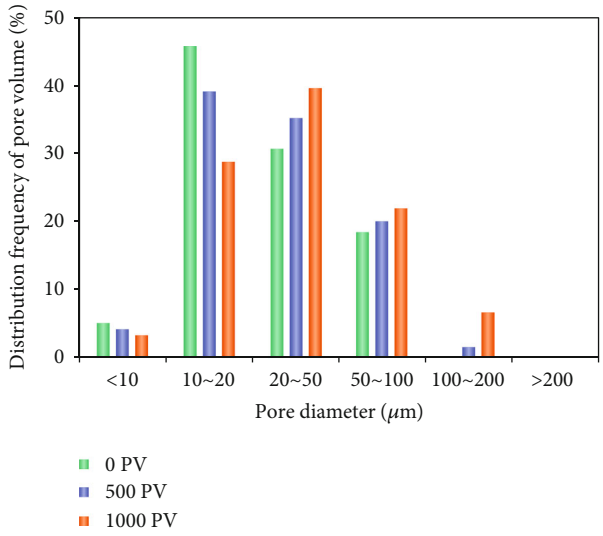

Figure 5: Volume distribution frequencies of pores of different sizes before and after gas displacement.

through CT scanning analysis, which is shown in Figure 3. And then, the distribution frequencies of the number and volume of pores of different sizes before and after gas displacement were calculated according to the 3D pore reconstruction analysis, and the results are shown in Figures 4 and 5. It suggested that the small pores and large pores changed in different ways. In general, the small pores outnumbered the large pores, but the volume of pores of different sizes was in normal distribution. With the gas injection, both the number and volume of the pores with a diameter less than 20 μm accounted for lower levels, while these of the larger pores accounted for higher levels. Among the pores, the number and volume distribution frequencies of the pores with a diameter from 20 μm to 50 μm increased significantly, and the pores with a diameter of more than

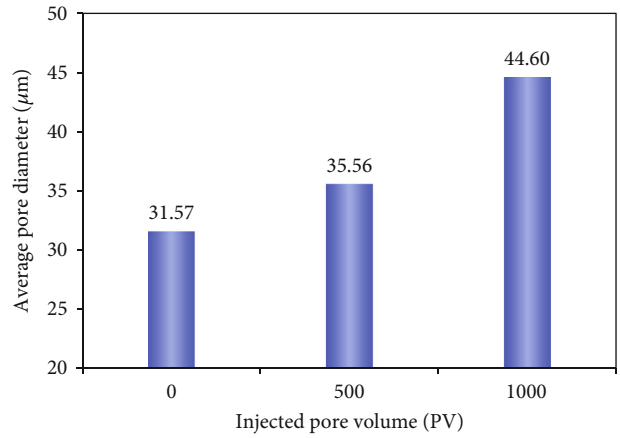

Figure 6: Average pore diameter before and after gas displacement.

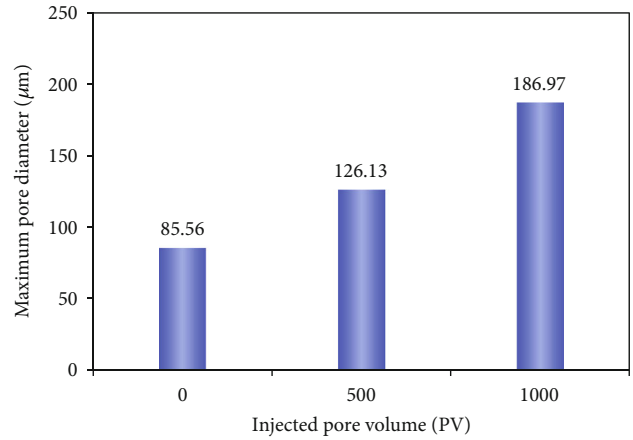

Figure 7: Maximum pore diameter before and after gas displacement.

100 μm came into existence after 500 PV gas was injected. It was calculated that the average and maximum pore diameter before and after gas displacement improved from 31.57 μm to 44.60 μm and 85.56 μm to 186.97 μm, respectively, as shown in Figures 6 and 7, which increased by 118.53% and 41.27%. Therefore, the continuous gas injection would lead to an apparent enlargement of pore size owing to the release and migration of unconsolidated sandstone particles [12, 14].

3.2. Effects of Gas Displacement on Pore-Throat Size. The number distribution frequencies of pore throats of different sizes before and after gas displacement were also calculated as shown in Figure 8 to investigate the pore-throat structure variations. It suggested that the number distribution frequencies of pore throats exhibited the same changes as these of the pores. The small pore throat outnumbered the large pore throat, and the number distribution frequencies of the pore throat with a diameter of less than 3 μm decreased from 56.2% to 49.7%, while these of the pore throat with a diameter of more than 3 μm increased that led to the increase of

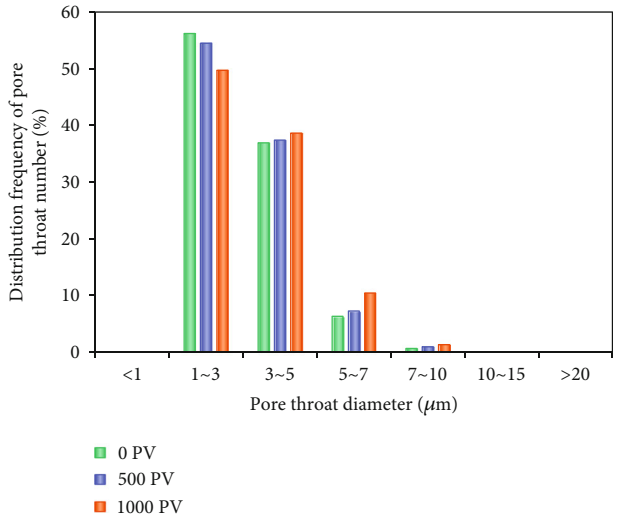

Figure 8: Number distribution frequencies of pore throats of different sizes before and after gas displacement.

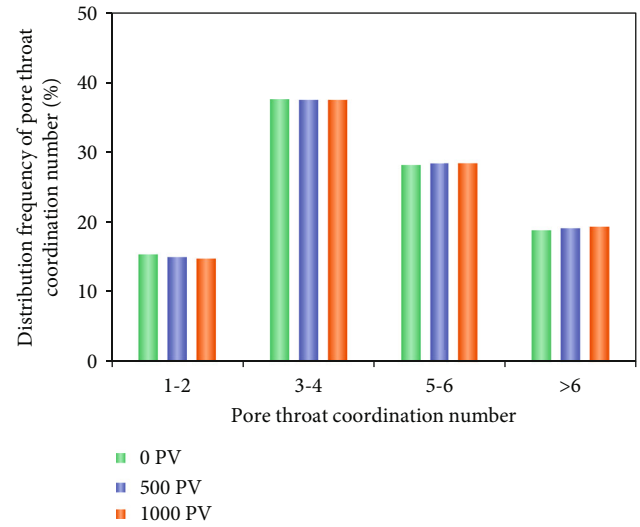

Figure 10: Distribution frequencies of pore-throat coordination number before and after gas displacement.

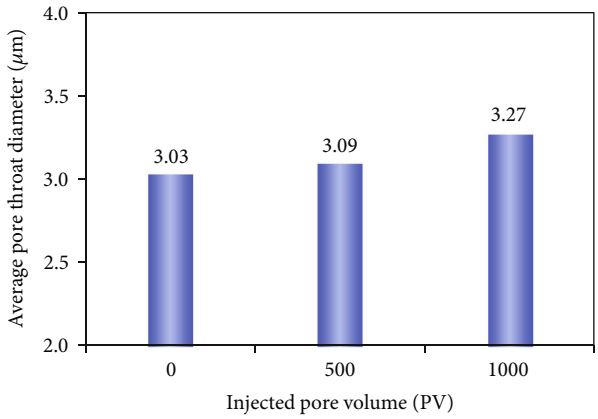

Figure 9: Average pore-throat diameter before and after gas displacement.

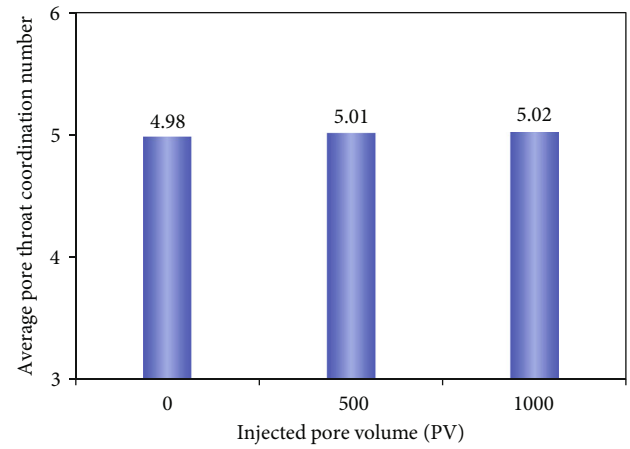

Figure 11: Average pore-throat coordination number before and after gas displacement.

the average pore-throat diameter before and after gas displacement from 3.03 μm to 3.27 μm as shown in Figure 9. The enlargement of the pore-throat diameter due to the rock mineral particle migration would enhance the pore connectivity and then improve the core permeability [36].

3.3. Effects of Gas Displacement on Pore-Throat Coordination Number. In order to investigate the pore-throat connectivity, the distribution frequencies of pore-throat coordination number before and after gas displacement were calculated as shown in Figure 10. And then, the average of the pore-throat coordination number was also calculated as shown in Figure 11. It suggested that the pore-throat coordination number from 3 to 6 accounted for the majority with a proportion of approximately 66%, and the average pore-throat coordination number came to be about 5. In terms of results before and after gas displacement, both the distribution and the average pore-throat coordination number changed slightly with few frequency declines of small pore-throat coordination number and few frequency increases of large pore-throat coordination number. The frequency decline might result from the particle blocking in the pore throat with a small diameter and low coordination number. Thus, it could be seen that the gas injection would enlarge the pore-throat diameter but have little effect on the coordination number between the pores and the throats.

3.4. Effects of Gas Displacement on Pore Connectivity. The pore structures of the CT core sample before and after gas displacement were reconstructed through CT scanning analysis, which is shown in Figure 12. And then, the porosities of both connected and isolated pores were calculated according to the 3D pore reconstruction analysis, and the results are shown in Figure 13. It suggested that the connected pores

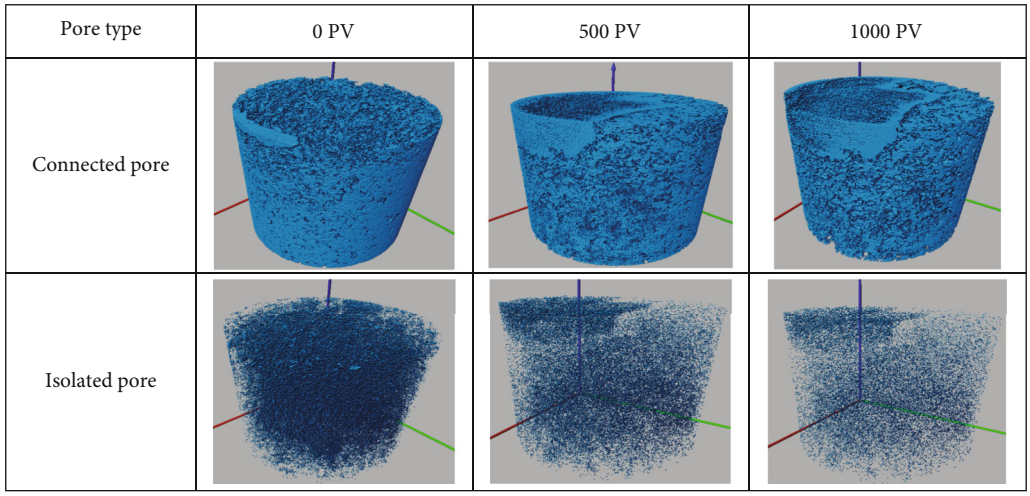

Figure 12: 3D structures of both connected and isolated pores before and after gas displacement.

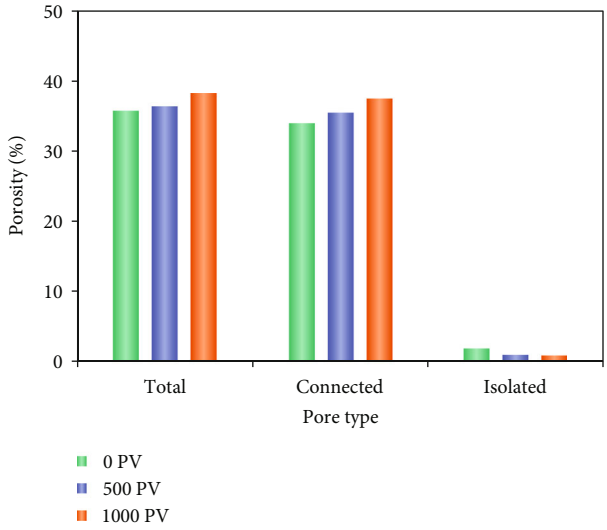

Figure 13: Porosities of both connected and isolated pores before and after gas displacement.

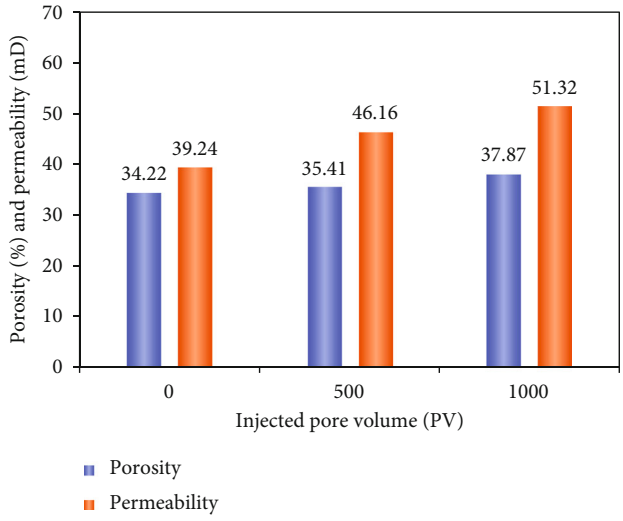

Figure 14: Porosity and permeability before and after gas displacement.

constituted the majority of the total pores with a proportion of more than 95%. After gas displacement, the porosity of the isolated pores declined, while the porosity of the connected pores increased by 10.3% from 33.9% to 37.4%, which brought about an increase of 2.5% from 35.7% to 38.2% in the total porosity. It can be seen from the results that the pore connectivity would be strengthened as a whole in spite of the pore blocking owing to the particle migration in the unconsolidated sandstone, and the reconnected pores outnumbered the reisolated pores in the gas injection process.

3.5. Effects of Gas Displacement on Porosity and Permeability. The core sample 2# was saturated by 3.0 wt.% KI solution and then flooded by gas (N_2) to 1000 PV. The porosity and permeability of the core sample were measured in different injected pore volumes, and the results are shown in Figure 14. It showed that both the porosity and permeability of the core sample increased apparently from 34.22% to 37.87% and 39.24 mD to 51.32 mD, respectively, which went up by 10.67% and 30.78%. The growth rate of the permeability was greater than that of the porosity [36]. The rock permeability was primarily based on the larger pores. The increase of the permeability of the core in unconsolidated sandstone mainly resulted from the enlargement of the pore and throat with larger sizes as well as the enhancement of the pore connectivity due to the particle migration as found above. Therefore, the porosity and permeability variations would not be neglected in the continuous gas displacement process in unconsolidated sandstone gas reservoirs, which could lead to the evident changes in the gas reserves as well as the well injectivity and productivity.

3.6. Effects of Gas Displacement on Relative Permeability. In gas reservoirs with edge and bottom water, gas and water

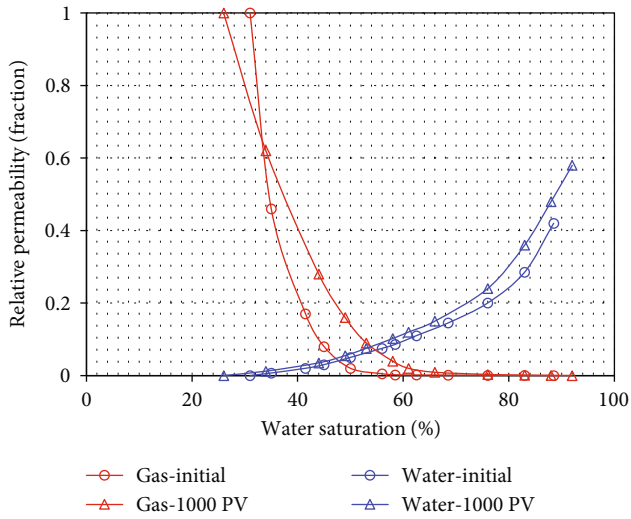

Figure 15: Gas and water relative permeability before and after gas displacement.

flow in the same place. The pore structure variations in the gas displacement process will necessarily result in the changes in phase relative permeability [37]. In order to investigate the gas and water flow principle, the gas-water relative permeability curves were measured before and after gas displacement as shown in Figure 15. From the measurement results, the initial gas and water relative permeability before gas injection were low sunken curves, and then, both the gas and water relative permeability increased after 1000 PV gas injection. The irreducible water saturation and the residual gas saturation dropped from 31.2% to 26.1% and 11.5% to 8.0%, which broadened the two-phase flow region. Additionally, the equal phase relative permeability point shifted to the right from 47.3% to 54.0%. The improvement of the phase relative permeability also got benefit from the enlargement of the pore and throat size as well as the enhancement of the pore connectivity. Compared with the water relative permeability, the gas relative permeability had a higher improvement.

4. Conclusions

In the current investigation, we present the quantitative results of pore structure and permeability variations during gas displacement in unconsolidated sandstone reservoirs through CT reconstruction analysis. Useful conclusions drawn from our research results are listed as follows:

(1) The continuous gas displacement would bring about an increase of more than 2.5% in the total porosity and enhance the pore connectivity, which primarily resulted from the enlargement of the pore and throat with larger sizes owing to the release and migration of clay and fine particles in unconsolidated sandstone reservoirs. The porosity of the connected pores constituted the majority of the total pores with a proportion of more than 95% and increased by 10.3% after gas displacement

(2) The continuous gas displacement not only improved the porosity and permeability from 34.22% to 37.87% and 39.24 mD to 51.32 mD, respectively, but also broadened the two-phase flow region. The irreducible water saturation and the residual gas saturation dropped, and the equal phase relative permeability point shifted to the right. Both the gas and water relative permeability could be enhanced after gas displacement in unconsolidated sandstone reservoirs

Abbreviations

CT: Computed tomography
NMR: Nuclear magnetic resonance
PV: Pore volume.

Data Availability

The data that support the findings of this study are available from the corresponding author, Zha Y., upon reasonable request.

Conflicts of Interest

The authors declare that they have no conflicts of interest.

Acknowledgments

This work was supported by the Hainan Branch and the Zhanjiang Branch of CNOOC China Limited, China.

References

[1] I. O. Stanley, "Gas-to-liquid technology: prospect for natural gas utilization in Nigeria," *Journal of Natural Gas Science & Engineering*, vol. 1, no. 6, pp. 190–194, 2009.

[2] J. A. Velasco, L. Lopez, M. Velásquez, M. Boutonnet, S. Cabrera, and S. Järås, "Gas to liquids: a technology for natural gas industrialization in Bolivia," *Journal of Natural Gas Science & Engineering*, vol. 2, no. 5, pp. 222–228, 2010.

[3] S. H. Mohr and G. M. Evans, "Long term forecasting of natural gas production," *Energy Policy*, vol. 39, no. 9, pp. 5550–5560, 2011.

[4] Y. C. Xu, W. H. Liu, P. Shen et al., "Carbon and hydrogen isotopic characteristics of natural gases from the Luliang and Baoshan basins in Yunnan Province, China," *Science in China Series D: Earth Sciences*, vol. 49, no. 9, pp. 938–946, 2006.

[5] C. H. Ou, X. Wang, C. C. Li, and Y. He, "Three-dimensional modelling of a multi-layer sandstone reservoir: the Sebei gas field, China," *Acta Geologica Sinica (English Edition)*, vol. 90, no. 1, pp. 209–221, 2016.

[6] C. Yan, J. Deng, Y. Cheng, X. Yan, J. Yuan, and F. Deng, "Rock mechanics and wellbore stability in Dongfang 1-1 gas field in South China Sea," *Geomechanics and Engineering*, vol. 12, no. 3, pp. 465–481, 2017.

[7] J. Deng, L. Wang, P. Li, and W. Zhao, "The critical pressure difference prediction of sand production in deepwater sandstone gas reservoirs," *Petroleum Science and Technology*, vol. 31, no. 19, pp. 1925–1932, 2013.

[8] J. Ren, L. Zhang, J. Ezekiel, S. Ren, and S. Meng, "Reservoir characteristics and productivity analysis of tight sand gas in

upper Paleozoic Ordos Basin China," *Journal of Natural Gas Science & Engineering*, vol. 19, pp. 244–250, 2014.

[9] R. Zhang, X. Shi, R. Zhu et al., "Critical drawdown pressure of sanding onset for offshore depleted and water cut gas reservoirs: modeling and application," *Journal of Natural Gas Science & Engineering*, vol. 34, pp. 159–169, 2016.

[10] Y. Wang, Y. Yang, K. Wang et al., "Changes in relative permeability curves for natural gas hydrate decomposition due to particle migration," *Journal of Natural Gas Science and Engineering*, vol. 84, article 103634, 2020.

[11] L. Jia, S. J. Peng, J. Xu, F. Yan, J. Chen, and B. Wu, "Investigation on gas drainage effect under different borehole layout via 3D monitoring of gas pressure," *Journal of Natural Gas Science and Engineering*, vol. 101, article 104522, 2022.

[12] T. Nguyen, A. Zeinijahromi, and P. Bedrikovetsky, "Fines-migration-assisted improved gas recovery during gas field depletion," *Journal of Petroleum Science and Engineering*, vol. 109, pp. 26–37, 2013.

[13] C. Wei, M. Zou, Y. Sun, Z. Cai, and Y. Qi, "Experimental and applied analyses of particle migration in fractures of coalbed methane reservoirs," *Journal of Natural Gas Science and Engineering*, vol. 23, pp. 399–406, 2015.

[14] A. Zeinijahromi, A. Vaz, and P. Bedrikovetsky, "Well impairment by fines migration in gas fields," *Journal of Petroleum Science & Engineering*, vol. 88-89, pp. 125–135, 2012.

[15] J. Q. Li, G. Zhao, Z. L. Qi et al., "Stress sensitivity of formation during multi-cycle gas injection and production in an underground gas storage rebuilt from gas reservoirs," *Petroleum Exploration and Development*, vol. 48, no. 4, pp. 968–977, 2021.

[16] T. Zhou, W. Yan, J. Su et al., "The influence of injected fluids on microscopic pore structures in the intersalt dolomitic shale oil reservoirs," *Geofluids*, vol. 2019, Article ID 4923173, 13 pages, 2019.

[17] Y. A. Sazali, W. M. L. Sazali, J. M. Ibrahim, G. Graham, and S. Gödeke, "Investigation of fines migration for a high-pressure, high-temperature carbonate gas reservoir offshore Malaysia," *Journal of Petroleum Exploration and Production Technology*, vol. 10, no. 6, pp. 2387–2399, 2020.

[18] W. Zhang, Q. Zhao, X. Guan, Z. Wang, and Z. Wang, "Experiment and model of conductivity loss of fracture due to fine-grained particle migration and proppant embedment," *Energies*, vol. 15, no. 7, p. 2359, 2022.

[19] Y. Hao, M. Smith, Y. Sholokhova, and S. Carroll, "CO_2-induced dissolution of low permeability carbonates. Part II: numerical modeling of experiments," *Advances in Water Resources*, vol. 62, no. 12, pp. 388–408, 2013.

[20] Z. Li, W. Zhang, Y. Tang, B. Li, Z. Song, and J. Hou, "Formation damage during alkaline-surfactant-polymer flooding in the Sanan-5 block of the Daqing oilfield, China," *Journal of Natural Gas Science & Engineering*, vol. 35, no. Part A, pp. 826–835, 2016.

[21] X. Huang and Y. P. Zhao, "Characterization of pore structure, gas adsorption, and spontaneous imbibition in shale gas reservoirs," *Journal of Petroleum Science & Engineering*, vol. 159, pp. 197–204, 2017.

[22] R. Jiang, W. Zhang, P. Zhao et al., "Characterization of the reservoir property time-variation based on 'surface flux' and simulator development," *Fuel*, vol. 234, pp. 924–933, 2018.

[23] S. Karimi and H. Kazemi, "Characterizing pores and pore-scale flow properties in middle Bakken cores," *SPE Journal*, vol. 23, no. 4, pp. 1343–1358, 2018.

[24] S. Karimi, H. Kazemi, and A. S. Gary, "Capillary pressure and wettability indications of middle Bakken core plugs for improved oil recovery," *SPE Reservoir Evaluation & Engineering*, vol. 22, no. 1, pp. 310–325, 2019.

[25] B. Cao, P. Wei, F. Tian et al., "Experimental investigation on cyclic huff-n-puff with surfactants based on complex fracture networks in water-wet oil reservoirs with extralow permeability," *Geofluids*, vol. 2021, Article ID 6898581, 10 pages, 2021.

[26] B. Cao, X. Lu, K. Xie et al., "The pore-scale mechanisms of surfactant-assisted spontaneous and forced imbibition in water-wet tight oil reservoirs," *Journal of Petroleum Science & Engineering*, vol. 213, article 110371, 2022.

[27] M. C. Ribeiro, J. G. Filgueiras, A. Souza, P. M. Vianna, R. B. V. de Azeredo, and R. Leiderman, "Image-based simulation of molecular diffusion on NMR pulsed-field gradient experiments: feasibility to estimate tortuosity and permeability of porous media," *Journal of Petroleum Science and Engineering*, vol. 219, article 111064, 2022.

[28] C. H. Arns, F. Bauget, A. Limaye et al., "Pore-scale characterization of carbonates using X-ray microtomography," *SPE Journal*, vol. 10, no. 4, pp. 475–484, 2005.

[29] R. Taghizadeh, K. Goshtasbi, A. K. Manshad, and K. Ahangari, "Geomechanical and thermal reservoir simulation during steam flooding," *Structural Engineering & Mechanics*, vol. 66, no. 4, pp. 505–513, 2018.

[30] Q. Cao, Y. Gong, T. Fan, and J. Wu, "Pore-scale simulations of gas storage in tight sandstone reservoirs for a sequence of increasing injection pressure based on micro-CT," *Journal of Natural Gas Science and Engineering*, vol. 64, pp. 15–27, 2019.

[31] J. Chaves and R. Moreno, "Low- and high-resolution X-ray tomography helping on petrophysics and flow-behavior modeling," *SPE Journal*, vol. 26, no. 1, pp. 206–219, 2021.

[32] A. Hanafy, H. A. Nasr-El-Din, and H. Zoya, "A novel method to assess stimulation of sandstone cores damaged by fines migration," *SPE Journal*, vol. 27, no. 1, pp. 682–704, 2022.

[33] H. Sun, J. Yao, Y.-c. Cao, D.-y. Fan, and L. Zhang, "Characterization of gas transport behaviors in shale gas and tight gas reservoirs by digital rock analysis," *International Journal of Heat and Mass Transfer*, vol. 104, pp. 227–239, 2017.

[34] S. Saraf and A. Bera, "A review on pore-scale modeling and CT scan technique to characterize the trapped carbon dioxide in impermeable reservoir rocks during sequestration," *Renewable and Sustainable Energy Reviews*, vol. 144, article 110986, 2021.

[35] C. Li, X. Li, S. Gao et al., "Experiment on gas-water two-phase seepage and inflow performance curves of gas wells in carbonate reservoirs: a case study of Longwangmiao Formation and Dengying Formation in Gaoshiti-Moxi block, Sichuan Basin, SW China," *Petroleum Exploration and Development*, vol. 44, no. 6, pp. 983–992, 2017.

[36] M. S. Sabo and L. E. Beckingham, "Porosity-permeability evolution during simultaneous mineral dissolution and precipitation," *Water Resources Research*, vol. 57, no. 6, pp. 1–15, 2021.

[37] C. Van der Land, R. Wood, K. J. Wu et al., "Modelling the permeability evolution of carbonate rocks," *Marine and Petroleum Geology*, vol. 48, no. 48, pp. 1–7, 2013.